Control Design: Swing-up 7

This chapter describes the different control methods investigated to swing up the pendulum to a point where the stabilising controller can take over, and keep the pendulum upright. As stated in the system requirements in **sections 3.1.1** and **3.1.2**, the objectives of the swing-up controller is to drive the cart in a motion such that the pendulum converges towards the heteroclinic orbits while keeping the cart at its reference position.

A theoretical approach based on LaSalle's invariance principle is presented from which two different control laws are derived; one in **section 7.1** based on the mechanical energy of the pendulum (omitting the cart) and one in **section 7.2**, which is based on the full system mechanical energy. These will be referred to as the *pendulum energy method* and *full energy method*, respectively.

Based on simulation results, the control laws are modified in **section 7.3** to meet the requirements, and a third method, a simpler variation to the method in **section 7.1** is introduced, which will be referred to as the *sign-based method*. Thus, three swing-up controllers are presented in this chapter and they will all be implemented and compared.

Note that all simulations presented in this chapter are done on the full nonlinear model.

7.1 Pendulum energy method

The following is based on [15].

In this section, a simple approach to the energy-based swing-up control will be derived. Consider the pendulum subsystem, with dynamics described by

$$\begin{aligned} 0 - B_p(\dot{\theta}) &= -m_p l\ddot{x}\cos\theta + m_p l^2\ddot{\theta} - m_p g l \sin\theta \\ &\Leftrightarrow J\ddot{\theta} = m_p l\ddot{x}\cos\theta + m_p g l\sin\theta - B_p(\dot{\theta}), \qquad J = m_p l^2 \end{aligned} \tag{7.1}$$

where $B_p(\dot{\theta})$ is the pendulum friction model. That is, the pendulum is described by the bottom row of **equation (4.17)**, page **15**.

Omitting the friction term in **equation (7.1)**, and letting the cart acceleration $\ddot{x}$ be considered the system input u, the equation becomes

$$J\ddot{\theta} = m_p l u\cos\theta + m_p g l\sin\theta \tag{7.2}$$

Since the input for this is an acceleration, but the real system requires a force, an approximate conversion from desired acceleration to force is presented in **section 7.1.1**. The mechanical energy for the pendulum, E_p, is given by the potential and kinetic energies, U_p and T_p, defined in **equation (4.11)**

and **equation (4.13)**, page **14**:

$$\begin{aligned} E_p &= T_p + U_p \\ &= \frac{1}{2} J\dot{\theta}^2 + m_p g l \cos\theta + u_{ref} \\ &= \frac{1}{2} J\dot{\theta}^2 + m_p g l \left(\cos\theta + 1\right) \end{aligned} \tag{7.3}$$

Taking the time derivative of the energy yields

$$\begin{aligned} \dot{E}_p &= J\dot{\theta}\ddot{\theta} - m_p g l \dot{\theta} \sin\theta \\ &= \left(m_p g l \sin\theta + m_p l u \cos\theta\right)\dot{\theta} - m_p g l \dot{\theta} \sin\theta \\ &= m_p l u \dot{\theta} \cos\theta \end{aligned} \tag{7.4}$$

From this equation, it is observed that the mechanical energy can be controlled with input u, and that control action is lost when $\theta = \pm\frac{\pi}{2}$ or $\dot{\theta} = 0$, i.e. when the pendulum is horizontal or not in motion. On the other hand, the control input is most effective when $\theta = \{0, \pm\pi\}$ and $\dot{\theta}$ is large.

In order to increase the energy of the pendulum, control input must be positive when $\dot{\theta}\cos\theta$ is positive. Recalling the definitions of the energy error in **section 6.2**, a control law following $\dot{\theta}\cos\theta$ and seeking to minimise the energy error is proposed

$$u = k_e(E^* - E_p)\dot{\theta}\cos\theta \tag{7.5}$$

where $k_e > 0$ is a controller gain.

Considering **theorem 6.1.2** (LaSalle's theorem), Ω is chosen as the set contained within the heteroclinic orbits in **figure 6.3**, i.e.

$$\Omega = \left\{ (\theta, \dot{\theta}) \mid 0 \leq \theta \leq 2\pi,\ -\sqrt{\frac{2g}{l}(1-\cos\theta)} \leq \dot{\theta} \leq \sqrt{\frac{2g}{l}(1-\cos\theta)} \right\} \tag{7.6}$$

Using the function

$$V_1(\theta, \dot{\theta}) = \frac{1}{2}(E^* - E_p)^2 = \frac{1}{2}\left((1-\cos\theta)g - \frac{1}{2}l\dot{\theta}^2\right)^2 \tag{7.7}$$

yields

$$\begin{aligned} \dot{V}_1(\theta, \dot{\theta}) &= (E^* - E_p)\left(\dot{E}^* - \dot{E}_p\right) \\ &= (E^* - E_p)\left(0 - m_p l u \dot{\theta}\cos\theta\right) \\ &= -(E^* - E_p) m_p l u \dot{\theta}\cos\theta \\ &= -(E^* - E_p) m_p l k_e (E^* - E_p)\dot{\theta}\cos\theta\dot{\theta}\cos\theta \\ &= -m_p l k_e \left((E^* - E_p)\dot{\theta}\cos\theta\right)^2 \leq 0 \end{aligned} \tag{7.8}$$

from which the set $\mathbb{E}$ is given by

$$\begin{aligned}\mathbb{E} &= \left\{(\theta,\dot{\theta}) \in \Omega \mid \dot{V}_1(\theta,\dot{\theta}) = 0\right\} \\ &= \left\{(\theta,\dot{\theta}) \in \Omega \mid \dot{\theta} = 0\right\} \cup \left\{(\theta,\dot{\theta}) \in \Omega \mid \dot{\theta} = \pm\sqrt{\frac{2g}{l}(1-\cos\theta)}\right\} \\ &= \mathbb{E}_1 \cup \mathbb{M}\end{aligned} \tag{7.9}$$

In this, $\mathbb{M}$ is the largest invariant set in $\mathbb{E}$, and thus from **theorem 6.1.2** (LaSalle's theorem) it follows that every solution starting in Ω approaches $\mathbb{M}$ as $t \to \infty$.

The control law in **equation (7.5)** does not include control of the cart position, and the cart must therefore be placed in the middle of the rail in order to avoid collision with the physical limits of the system.

A simulation using the control law in **equation (7.5)** is shown in **figure 7.1** and **figure 7.2** with $k_e = 0.5$

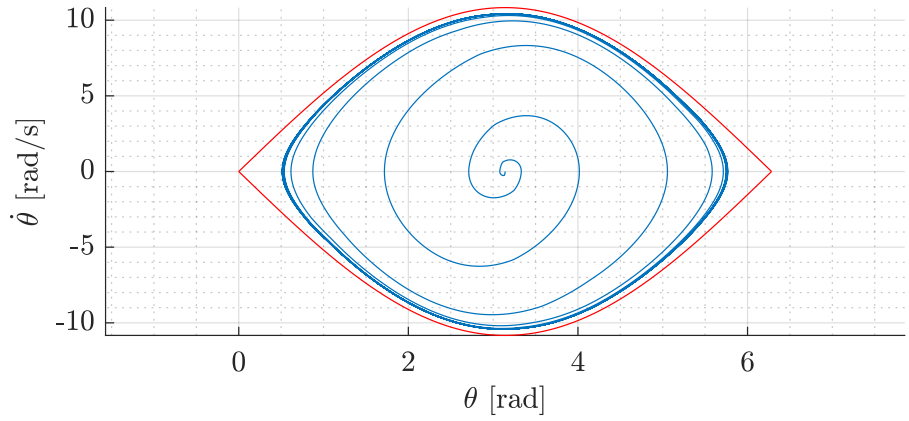

Figure 7.1: *Phase plot(blue) of a simulation using the derived control law and the full system model. The heteroclinic orbits(red) are added as reference. Simulation is done on the full nonlinear model.*

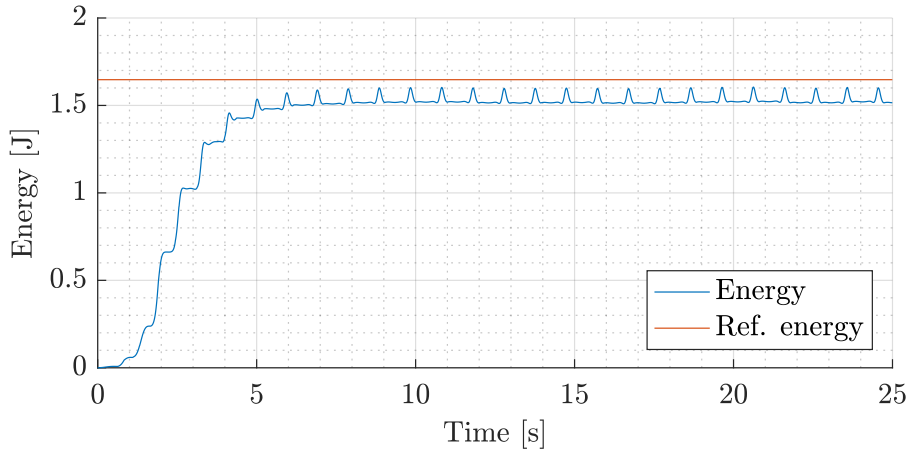

Figure 7.2: *Pendulum energy when simulating the full model using the derived control law in **equation (7.5)**. Simulation is done on the full nonlinear model.*

It is seen that the pendulum does not fully reach the heteroclinic orbits, thus the control law is insufficient. In order to remedy this, a different approach will be considered in **section 7.2**.

7.1.1 Cart acceleration to force

When considering the cart acceleration as the pendulum subsystem input, and deriving a control law based on this, the controller output must be converted to a force.

From **equation (4.17)** on page **15**, the relation between F and $\ddot{x}$ is

$$F = (m_c + m_p)\ddot{x} - m_p l \cos\theta\ddot{\theta} + m_p l \sin\theta\dot{\theta}^2 \tag{7.10}$$

when omitting the cart friction.

This relation is used to compute the force to apply to the system from the control signal u by replacing $\ddot{x}$ with u and using θ, $\dot{\theta}$ and $\ddot{\theta}$ from the EKF.

7.2 Full energy method

The following is based on [16, 17].

Instead of considering just the pendulum energy, this method considers the energy of the entire system, attempting to include control of the cart in the derivation of the control law. The full system energy is defined using the the potential energy of the pendulum, U_p, from **equation (4.11)** on page **14** and inertia matrix from **equation (4.17)** on page **15**.

$$\begin{aligned} E &= \frac{1}{2}\dot{\mathbf{q}}^T\mathbf{M}(\theta)\dot{\mathbf{q}} + U_p \\ &= \frac{1}{2}\begin{bmatrix}\dot{x} & \dot{\theta}\end{bmatrix}\begin{bmatrix} m_c + m_p & -m_p l\cos\theta \\ -m_p l\cos\theta & m_p l^2\end{bmatrix}\begin{bmatrix}\dot{x} \\ \dot{\theta}\end{bmatrix} + m_p g l(\cos\theta + 1) \\ &= \frac{1}{2}\dot{x}^2(m_c + m_p) + \frac{1}{2}\dot{\theta}^2 m_p l^2 - \dot{x}\dot{\theta} m_p l\cos\theta + m_p g l(\cos\theta + 1) \end{aligned} \tag{7.11}$$

Furthermore, the dynamics presented in **equation (4.17)** are considered, using the generalised coordinate to express the accelerations

$$\mathbf{M}(\theta)\ddot{\mathbf{q}} = -\mathbf{C}(\theta,\dot{\theta}) - \mathbf{G}(\theta) + \boldsymbol{\tau} - \mathbf{B}(\dot{\theta}), \qquad \boldsymbol{\tau} = [u \quad 0]^T \tag{7.12}$$

As in **section 7.1**, the pendulum friction is omitted, effectively setting $\mathbf{B} = \mathbf{0}$. The time derivative of

equation (7.11) yields

$$\begin{aligned}
\dot{E} &= \frac{1}{2}\ddot{\mathbf{q}}^T\mathbf{M}(\theta)\dot{\mathbf{q}} + \frac{1}{2}\dot{\mathbf{q}}^T\dot{\mathbf{M}}(\theta)\dot{\mathbf{q}} + \frac{1}{2}\dot{\mathbf{q}}^T\mathbf{M}(\theta)\ddot{\mathbf{q}} + \dot{U}_p \\
&= \dot{\mathbf{q}}^T\mathbf{M}(\theta)\ddot{\mathbf{q}} + \frac{1}{2}\dot{\mathbf{q}}^T\dot{\mathbf{M}}(\theta)\dot{\mathbf{q}} + \dot{\mathbf{q}}^T\mathbf{G}(\theta), \qquad \frac{\partial U_p}{\partial \mathbf{q}} = \dot{\mathbf{q}}^T\mathbf{G}(\theta) \\
&= \dot{\mathbf{q}}^T\Big(\boldsymbol{\tau} - \mathbf{C}(\theta,\dot{\theta}) - \mathbf{G}(\theta)\Big) + \frac{1}{2}\dot{\mathbf{q}}^T\dot{\mathbf{M}}(\theta)\dot{\mathbf{q}} + \dot{\mathbf{q}}^T\mathbf{G}(\theta) \\
&= \dot{\mathbf{q}}^T\boldsymbol{\tau} - \dot{\mathbf{q}}^T\mathbf{G}(\theta) + \dot{\mathbf{q}}^T\mathbf{G}(\theta) - \dot{\mathbf{q}}^T\mathbf{C}(\theta,\dot{\theta}) + \frac{1}{2}\dot{\mathbf{q}}^T\dot{\mathbf{M}}(\theta)\dot{\mathbf{q}} \\
&= \dot{\mathbf{q}}^T\boldsymbol{\tau} - \begin{bmatrix}\dot{x} & \dot{\theta}\end{bmatrix}\begin{bmatrix} m_p l\sin\theta\dot{\theta}^2 \\ 0\end{bmatrix} + \frac{1}{2}\begin{bmatrix}\dot{x} & \dot{\theta}\end{bmatrix}\begin{bmatrix} 0 & m_p l\sin\theta\dot{\theta} \\ m_p l\sin\theta\dot{\theta} & 0\end{bmatrix}\begin{bmatrix}\dot{x} \\ \dot{\theta}\end{bmatrix} \\
&= \dot{x}u
\end{aligned} \tag{7.13}$$

The following function is then proposed, including the cart position and velocity, from which a control law is found inspired by the Lyapunov redesign approach:

$$V_2(\mathbf{x}) = \frac{k_e}{2}(E^* - E)^2 + \frac{k_v}{2}\dot{x}^2 + \frac{k_x}{2}(x^* - x)^2 \tag{7.14}$$

where k_e, k_v, and k_x are positive constants, E^* and x^* are energy and position references. Taking the time derivative yields

$$\begin{aligned}
\dot{V}_2(\mathbf{x}) &= -k_e(E^* - E)\dot{E} + k_v\dot{x}\ddot{x} - k_x(x^* - x)\dot{x} \\
&= -k_e(E^* - E)\dot{x}u + k_v\dot{x}\ddot{x} - k_x(x^* - x)\dot{x} \\
&= \dot{x}\Big(-k_e(E^* - E)u + k_v\ddot{x} + k_x(x^* - x)\Big)
\end{aligned} \tag{7.15}$$

Inserting the equation of $\ddot{x}$ from **equation (4.40)** on page **21**, the derivative extends to

$$\dot{V}_2(\mathbf{x}) = \dot{x}\bigg(u\Big(-k_e(E^* - E) + k_v\acute{\alpha}(\theta)\Big) + k_v\acute{\beta}(\theta,\dot{\theta}) - k_x(x^* - x)\bigg) \tag{7.16}$$

Where

$$\acute{\alpha}(\theta) = \frac{1}{m_c + m_p\sin^2\theta} \tag{7.17}$$

$$\acute{\beta}(\theta,\dot{\theta}) = \frac{m_p\sin\theta(-l\dot{\theta}^2 + g\cos\theta)}{m_c + m_p\sin^2\theta} \tag{7.18}$$

Based on **equation (7.16)** a control law is proposed such that

$$u\Big(-k_e(E^* - E) + k_v\acute{\alpha}(\theta)\Big) + k_v\acute{\beta}(\theta,\dot{\theta}) - k_x(x^* - x) = -k_d\dot{x} \tag{7.19}$$

Where k_d is a positive constant. The control law is derived by isolating u in **equation (7.19)**, which yields

$$u = \frac{-k_d\dot{x} + k_x(x^* - x) - k_v\acute{\beta}(\theta,\dot{\theta})}{-k_e(E^* - E) + k_v\acute{\alpha}(\theta)} \tag{7.20}$$

Inserting **equation (7.20)** into **equation (7.16)** results in

$$\dot{V}_2(\mathbf{x}) = -k_d\dot{x}^2 \leq 0 \tag{7.21}$$

In order to apply **theorem 6.1.2** (LaSalle's theorem) to **equation (7.21)** based on the set Ω in **equation (7.6)**, the coordinate transformation

$$T = \begin{bmatrix} 0 & 1 & 0 & 0 \\ 0 & 0 & 0 & 1 \\ 1 & 0 & 0 & 0 \\ 0 & 0 & 1 & 0 \end{bmatrix} \tag{7.22}$$

is used, which yields the transformed state vector $\tilde{\mathbf{x}} = [\theta \quad \dot{\theta} \quad x \quad \dot{x}]^T$. Then, the fourth-dimensional set Ω_4 can be defined as

$$\begin{aligned} \Omega_4 &= \Omega \times [x_{min}, x_{max}] \times [\dot{x}_{min}, \dot{x}_{max}] \\ &= \Omega \times [0,\ l_{rail} - w_{cart}] \times [\dot{x}_{min}, \dot{x}_{max}] \end{aligned} \tag{7.23}$$

From **equation (7.23)** the set $\mathbb{E}_4$ is defined as

$$\mathbb{E}_4 = \left\{ \tilde{\mathbf{x}} \in \Omega_4 \mid \dot{V}_2(\tilde{\mathbf{x}}) = 0 \right\} \tag{7.24}$$

As in **section 7.1**, it is desired to find the largest invariant set in $\mathbb{E}_4$, denoted $\mathbb{M}_4$, such that it follows from **theorem 6.1.2** (LaSalle's theorem) that every solution starting in Ω_4 approaches $\mathbb{M}_4$ as $t \to \infty$.

Simulations shows, as the one depicted in **figure 7.3**, that the largest invariant set is

$$\mathbb{M}_4 = \left\{ \tilde{\mathbf{x}} \in \Omega_4 \mid \dot{\theta} = \pm\sqrt{\frac{2g}{l}(1 - \cos\theta)}, \dot{x} = 0, x = x^* \right\} \tag{7.25}$$

which corresponds to the bright red orbit. The set relates to $\mathbb{E}_4$ by

$$\mathbb{E}_4 = \mathbb{M}_4 \cup \mathbb{E}_4 \setminus \mathbb{M}_4 \tag{7.26}$$

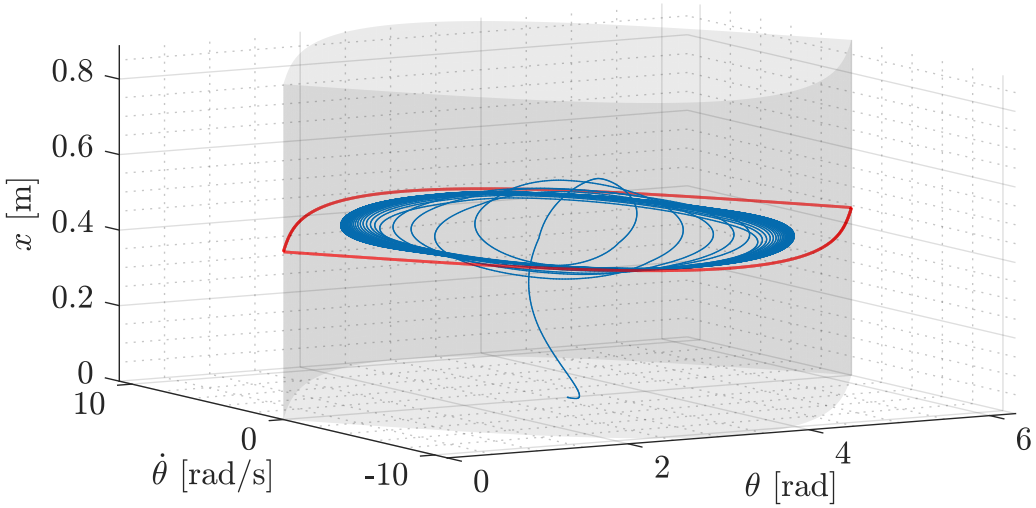

Figure 7.3: *Phase plot(blue) of the derived control law simulated on the full nonlinear model. The red orbit corresponds to the set $\mathbb{M}_4$. The shaded cylinder represents the set $\mathbb{M}_4$ where $0 \leq x^* \leq l_{rail} - w_{cart}$.*

The simulation is performed on the full nonlinear model, using the following gains $k_x = 12$, $k_d = 1$, $k_v = 8.3$, and $k_e = 1$.

As the simulations in **figure 7.1** and **figure 7.3** show, neither the pendulum energy method nor the full energy method manage to reach the heteroclinic orbits. Therefore, other approaches must be considered to ensure this, such that the stabilising controller can be enabled and stabilise the pendulum.

7.3 Heuristic swing-up control design

The results in **section 7.1** and **section 7.2** indicate that the control laws are not able to reach the heteroclinic orbits. This section continues on the basis of these results, but with a heuristic approach and only concern reaching the heteroclinic orbits by modifying the control laws.

In **section 7.3.1** the full energy method is reconsidered by adding an integral term such that it reaches the energy reference and heteroclinic orbits. The pendulum energy method's control law is expanded to include the cart position, and an integral term is also added, which is explained **section 7.3.2**. In **section 7.3.3** the sign-based method is presented, which is, as mentioned, a simpler variation of the method presented in **section 7.1**.

Adding and tuning the integral terms must be done carefully to avoid overshooting the energy reference before the stabilising controller takes over.

7.3.1 Full energy method

This section is based on the results presented in **section 7.1** (Full energy method).

Considering the simulation data of the phase plot in **figure 7.3**, the energy over time is shown in **figure 7.4**.

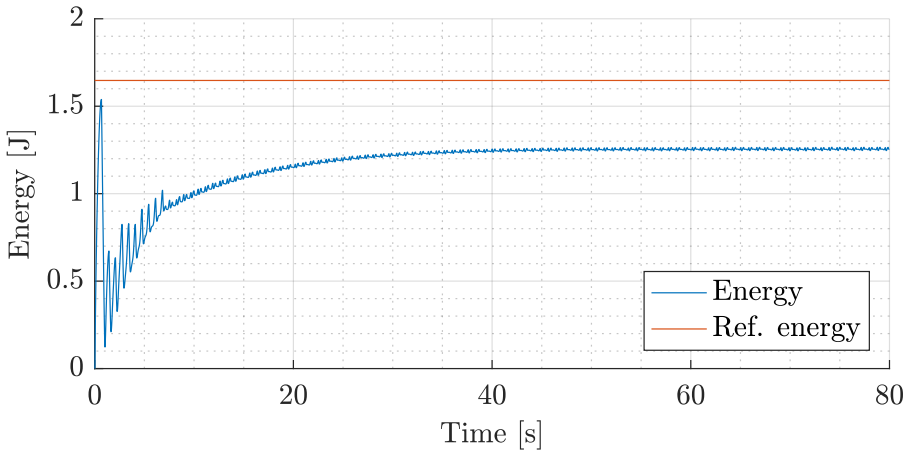

Figure 7.4: *System energy when using the control derived in the Full energy method in **section 7.2**, simulated on the full model.*

Here, it is seen that it does not reach the reference energy, but settles with a steady-state error. In order to eliminate this error, an integral term is added to the existing control law in **equation (7.20)**,

such that

$$u = \frac{-k_d\dot{x} + k_x(x^* - x) - k_v\acute{\beta}(\theta, \dot{\theta})}{-k_e(E^* - E) + k_v\acute{\alpha}(\theta)} + \dot{\theta}\cos\theta k_i \int_0^t e(\tau)dt \tag{7.27}$$

where $e(\tau) = E^* - E$ is the integrated energy error from time $t = 0$ until t, and k_i is a positive constant. The term $\dot{\theta}\cos\theta$ originates from [15], where it is shown that it maximises the efficiency of the control signal at the most appropriate time thus not working against the existing control signal.

Using $k_x = 12, k_d = 1, k_v = 8.3, k_e = 1$, and $k_i = 0.012$, **figure 7.5** shows that the heteroclinic orbits is reached, but also exceeded. **Figure 7.5** shows the phase, and the trajectory indicates that

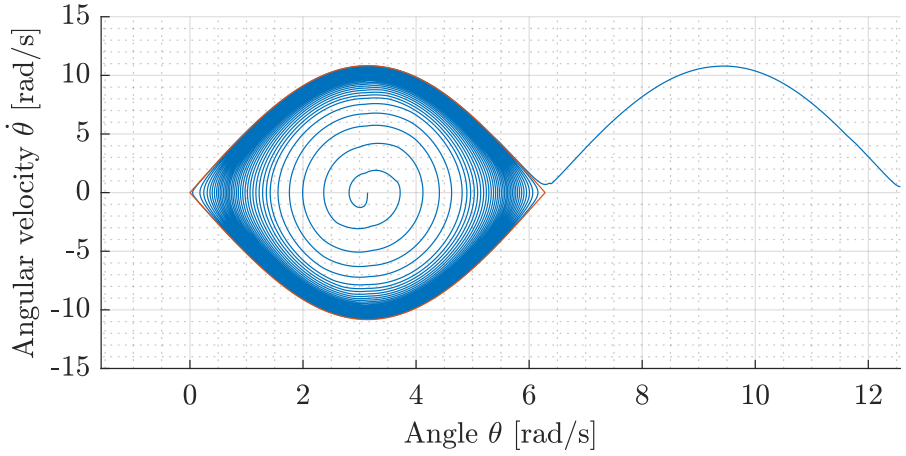

Figure 7.5: *Heteroclinic orbits(red) reached using the control law in **equation (7.27)**. The phase(blue) exceeds the heteroclinic orbits. Simulated on the full model.*

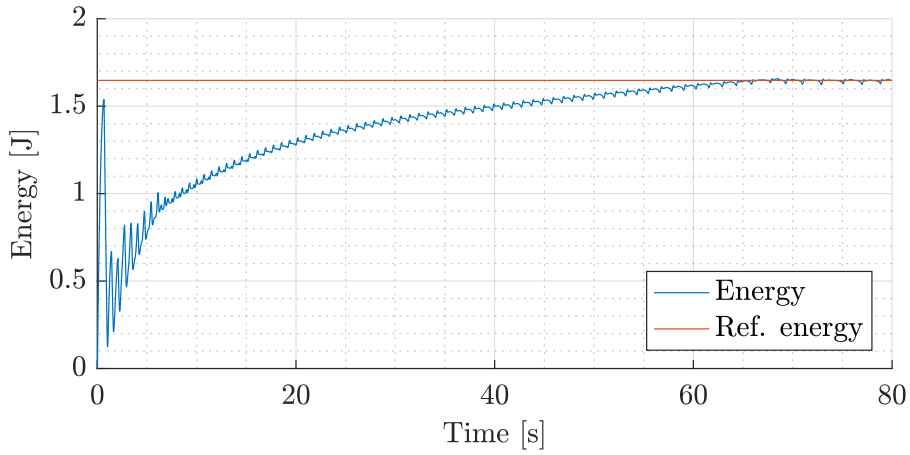

Figure 7.6: *Energy reference reached using the control law in **equation (7.27)**. Simulated on the full model.*

the pendulum does a full revolution, and therefore leaves the heteroclinic orbits between $\theta = 0$ and $\theta = 2\pi$.

Figure 7.6 shows the system energy, which settles slowly but without overshooting. Increasing the integral gain improves the energy rise time, however it also introduce overshoot, and gains are therefore kept as is.

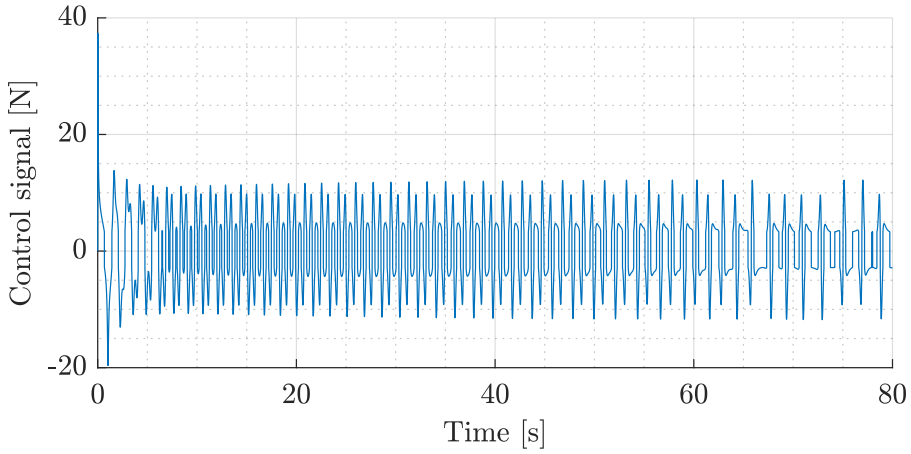

Figure 7.7: *The control signal of **equation (7.27)** when simulated on the full model.*

Finally, the k_v and k_e gains have been chosen systematically, based on the denominator in **equation (7.27)**. To avoid singularities, the following relation can be established:

$$0 \neq -k_e(E^* - E) + \frac{k_v}{m_c + m_p \sin^2\theta} \tag{7.28}$$

$$\frac{k_v}{k_e} \neq (E^* - E)(m_c + m_p \sin^2\theta) \tag{7.29}$$

Inspecting the maximum value of the right hand side, i.e. when $\sin^2\theta = 1$, and using the inequality $E^* - E \leq 2m_p gl$, gives

$$\frac{k_v}{k_e} \geq 8.2381 \tag{7.30}$$

The inequality is achieved by setting $k_v = 8.3$ and $k_e = 1$. The other gains are chosen iteratively during the design process.

7.3.2 Pendulum energy method

This section continues based on the results shown in **section 7.1** (Pendulum energy method). The results presented in **figure 7.1** do not include control of the cart position, and it is therefore required to start in the middle of the rail. In order to reach a reference position for the cart, and keep it within the limits of the physical setup, a proportional control is added to the control law defined in **equation (7.5)**, such that

$$u = k_e(E^* - E_p)\dot{\theta}\cos\theta + k_c(x^* - x) \tag{7.31}$$

Based on the results in **section 7.1**, where the pendulum energy settles with a steady-state error, an integral term on the energy error is added, i.e.

$$\begin{aligned} u &= k_e(E^* - E_p)\dot{\theta}\cos\theta + k_c(x^* - x) + k_i\dot{\theta}\cos\theta \int_0^t e_p(\tau)d\tau \\ &= \left(k_e(E^* - E_p) + k_i \int_0^t e_p(\tau)d\tau\right)\dot{\theta}\cos\theta + k_c(x^* - x) \end{aligned} \tag{7.32}$$

where the integral error is defined as $e_p(\tau) = E^* - E_p$, from time 0 until time t.

A simulation using this revised control law are shown in **figures 7.8** and **7.9** with $k_e = 0.5$, $k_i = 0.02$ and $k_c = 1$, chosen iteratively.

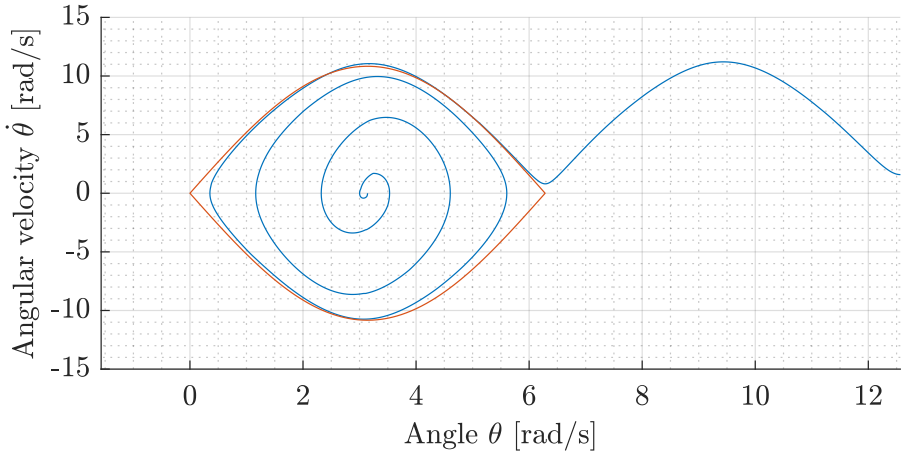

Figure 7.8: *Pendulum phase plot(blue) for pendulum energy control with integral action on the full model. The heteroclinic orbits(red) are also shown.*

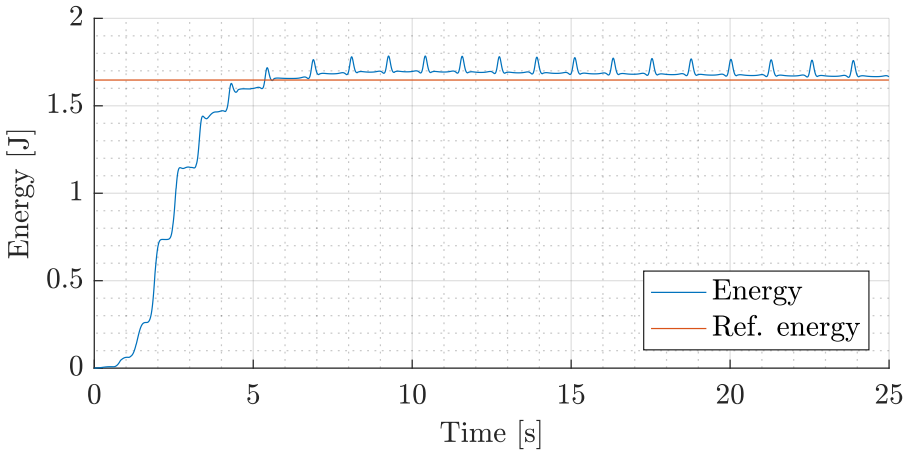

Figure 7.9: *Pendulum energy for pendulum energy control with integral action. Simulated on the full model.*

This shows that the mechanical energy reference is exceeded by a small margin, and the pendulum does several full revolutions once this happens.

The controller output for the simulation is shown in **figure 7.10**.

Tests with the value of k_i have shown that setting it too high will produce an overshoot, after which the energy will slowly decrease to the reference. Setting it too low will lower the rate at which the steady state error is corrected.

In general, this control approach utilises a simple expression for computing the system input, yet it struggles with reaching the energy reference, and relies on integral action to reach the value. The gain on the integral action is very sensitive, but a small overshoot is not an issue, as the stabilising control will take over once both the energy and angle criteria are met, as described in **section 6.4**.

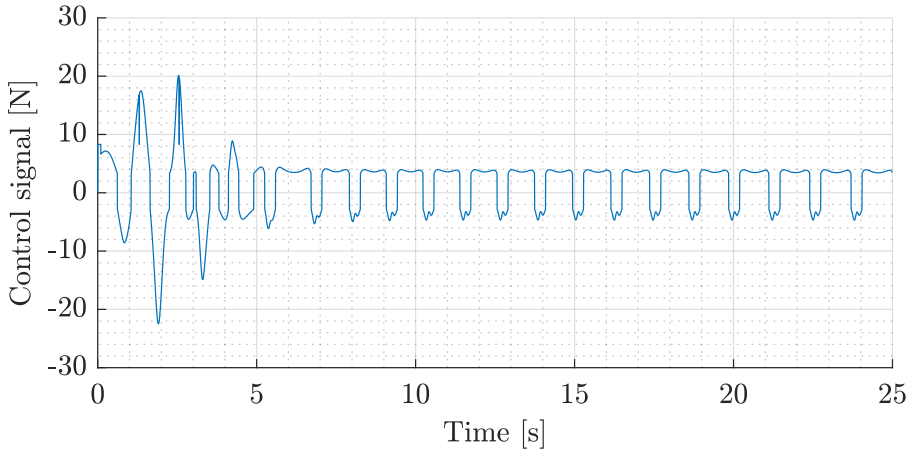

Figure 7.10: *Controller output from the pendulum energy method with integral action.*

7.3.3 Sign-based method

The following is based on [15].

As an alternative to the control law proposed in **equation (7.5)**, [15] suggests maximising the control input in order to increase the rate at which the energy error converges to zero.

This is achieved by defining a maximum control signal constant, u_{max}, and the control law

$$u = u_{max} \operatorname{sgn}\Big((E^* - E_p)\dot{\theta}\cos\theta\Big) \tag{7.33}$$

which drives $|E^* - E_p|$ towards zero.

Considering the function in **equation (7.7)**,

$$V_3(\mathbf{x}) = V_1(\mathbf{x}) = \frac{1}{2}(E^* - E_p)^2 = \frac{1}{2}\left((1-\cos\theta)g - \frac{1}{2}l\dot{\theta}^2\right)^2 \tag{7.34}$$

yields

$$\begin{aligned}\dot{V}_3(\mathbf{x}) &= -(E^* - E_p)m_p l u \dot{\theta}\cos\theta \\ &= -(E^* - E_p)m_p l u_{max} \operatorname{sgn}\Big((E^* - E_p)\dot{\theta}\cos\theta\Big)\dot{\theta}\cos\theta\end{aligned} \tag{7.35}$$

Recalling that $\operatorname{sgn}(0) = 0$, proving convergence towards a set using **theorem 6.1.2** (LaSalle's theorem) yields the sets defined in **equation (7.9)**.

The control law in **equation (7.33)** will cause chattering around $(E^* - E_p)\dot{\theta}\cos\theta = 0$. Therefore, the $\operatorname{sgn}(\cdot)$ can be replaced by e.g. a saturation function. Chattering will occur shortly when the pendulum changes direction, and as θ approaches zero. However, as this project relies on a different controller for stabilising the pendulum in the vicinity of $\theta = 0$, this is not expected to be an issue.

Additionally, for the control of the cart position, **equation (7.33)** can be extended to

$$u = u_{max} \operatorname{sgn}\Big((E^* - E_p)\dot{\theta}\cos\theta\Big) + k_c(x^* - x) \tag{7.36}$$

A simulation of the full nonlinear system with this control law is shown in **figures 7.11** and **7.12**, with $u_{max} = 1$ and $k_x = 1$.

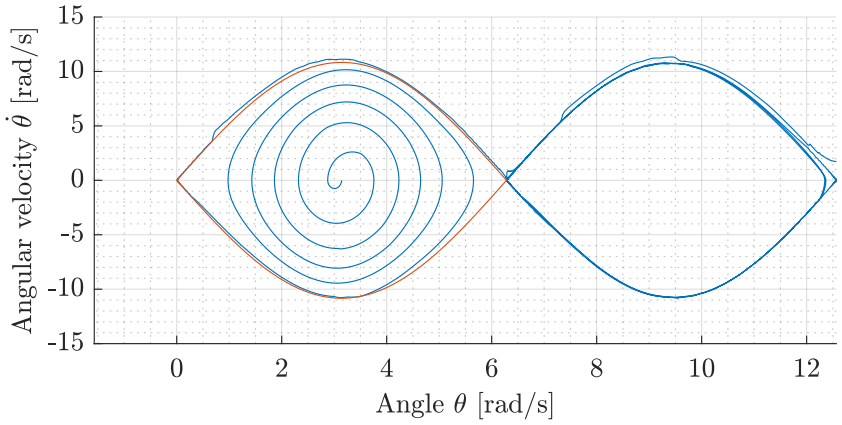

Figure 7.11: *Pendulum phase plot(blue) for the sign-based method, simulated on the full model. The heteroclinic orbits(red) are shown.*

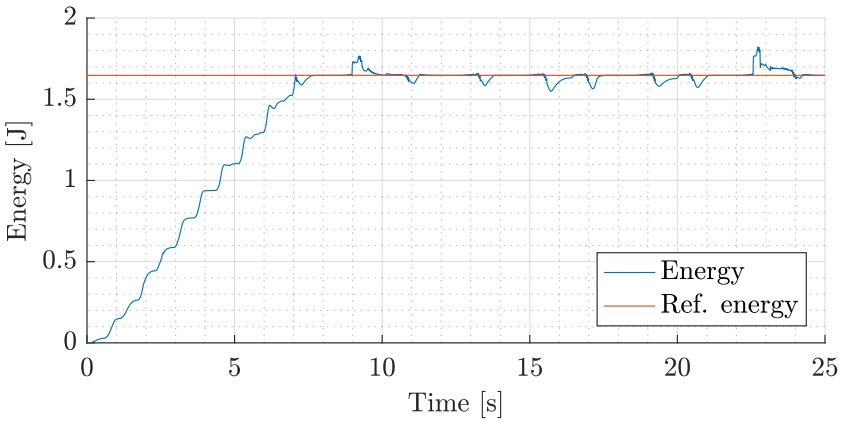

Figure 7.12: *Pendulum energy for the sign-based method, simulated on the full model.*

They show that this control law quickly increases the energy of the pendulum and settles very close to the reference. The system energy is generally kept, but temporarily exceeds the reference at $t \approx 9$ s, causing the pendulum to do a full revolution, as is seen on the phase plot. Additionally, this method does not require integral action.

The corresponding controller output in shown in **figure 7.13**. Here, it is evident how the $\operatorname{sgn}(\cdot)$

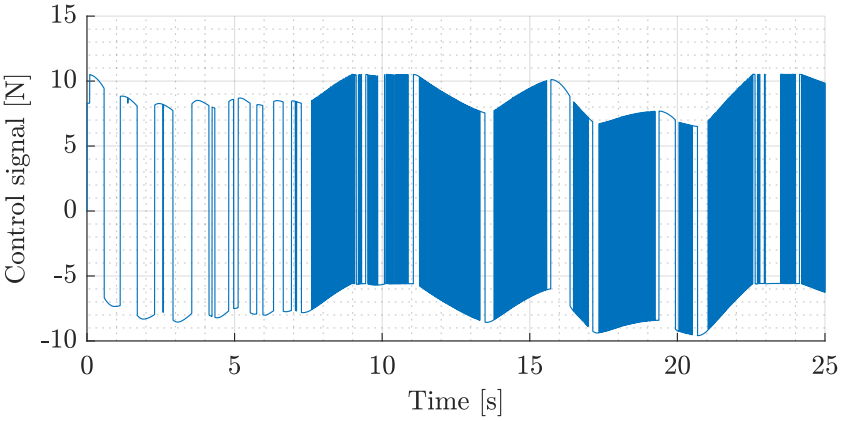

Figure 7.13: *Control output of the sign-based method.*

affects the controller output. At $t \approx 7.5$ s, when the energy reference is met, the chattering occurs.

Control Design: Stabilisation 8

This chapter presents the different control methods which will stabilise the pendulum in the upright position while keeping the cart in its reference position.

Three different controller types are considered. **Section 8.1** presents a cascade coupled Proportional-Integral-Derivative (PID) control scheme using decoupled dynamics of the pendulum and cart. In **section 8.2** an Linear-Quadratic-Gaussian (LQG) control scheme is derived, and lastly a nonlinear Sliding-Mode Controller (SMC) is derived in **section 8.3**. Thus three stabilising controllers will be designed, implemented, and compared.

Recall that the friction term of the cart is omitted, and added as a feedforward term, as described in **section 6.3**.

Note that all simulations presented in this chapter are done on the full nonlinear model.

8.1 Proportional-Integral-Derivative control

An PID control scheme has been developed to stabilize the pendulum and keep the cart at a desired position. Since the PID controller itself is only able to control one variable, two PID controllers have been coupled to control the x and θ variables.

Recall the dynamics defined in **equation (4.17)**:

$$\begin{bmatrix} u \\ 0 \end{bmatrix} - \mathbf{B}(\dot{x}, \dot{\theta}) = \underbrace{\begin{bmatrix} m_c + m_p & -m_p l \cos\theta \\ -m_p l \cos\theta & m_p l^2 \end{bmatrix}}_{\mathbf{M}(\theta)} \begin{bmatrix} \ddot{x} \\ \ddot{\theta} \end{bmatrix} + \underbrace{\begin{bmatrix} m_p l \sin\theta \dot{\theta}^2 \\ 0 \end{bmatrix}}_{\mathbf{C}(\theta, \dot{\theta})} + \underbrace{\begin{bmatrix} 0 \\ -m_p g l \sin\theta \end{bmatrix}}_{\mathbf{G}(\theta)} \tag{8.1}$$

This is simplified using the small angle approximation technique, such that

$$\begin{aligned} u &= \mathbf{M}_{(1,1)}\ddot{x} + \mathbf{M}_{(1,2)}\ddot{\theta} + \mathbf{C} \\ u &= (m_c + m_p)\ddot{x} - m_p l\ddot{\theta} + m_p l\theta\dot{\theta}^2 \end{aligned} \tag{8.2}$$

and

$$\begin{aligned} -\mathbf{B}_p(\dot{\theta}) &= \mathbf{M}_{(2,1)}\ddot{x} + \mathbf{M}_{(2,2)}\ddot{\theta} + \mathbf{G} \\ -v_p\dot{\theta} &= -m_p l\ddot{x} + m_p l^2\ddot{\theta} - m_p g l\theta \end{aligned} \tag{8.3}$$

In order to create two decoupled transfer functions, the terms $-m_p l\ddot{\theta} + m_p l\theta\dot{\theta}^2$ are considered as disturbances in **equation (8.2)** and thus removed. The Laplace transform of this yields

$$u = (m_c + m_p)xs^2 \tag{8.4}$$

and a transfer function is then found to be

$$H_c(s) = \frac{x(s)}{u(s)} = \frac{1}{(m_c + m_p)s^2} \tag{8.5}$$

Viewing the cart acceleration as an input, i.e. $u_2 = \ddot{x}$, in **equation (8.3)**, the Laplace transform yields

$$-v_p\theta s = -m_p l u_2 + m_p l^2 \theta s^2 - m_p g l \theta \tag{8.6}$$

and a transfer function for the pendulum is found to be

$$H_p(s) = \frac{\theta(s)}{u_2(s)} = \frac{m_p l}{m_p l^2 s^2 + v_p s - m_p g l} \tag{8.7}$$

The control scheme is depicted in **figure 8.1**.

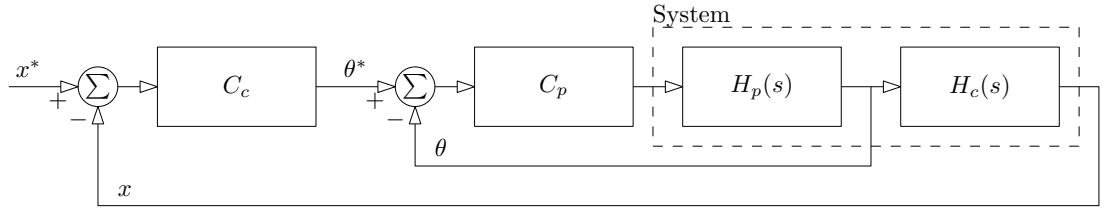

Figure 8.1: *PID control scheme. One PID, C_c, to control the cart position, the output is fed as a reference to the next PID controller, C_p, which controls the pendulum angle. The system is represented by the two transfer functions $H_p(s)$ and $H_c(s)$.*

Where C_c and C_p are the PID controllers on the form

$$C = \frac{K_d s^2 + K_p s + K_i}{s} \tag{8.8}$$

Where K_p, K_i, and K_d are gains for each of the control laws found iteratively and shown in **table 8.1**.

	C_c	C_p
K_p	0.2	112
K_i	0.03	15
K_d	0.15	15

Table 8.1: *Gains for the two PID controllers.*

When designing a cascade control scheme, the inner loop must be faster than the outer loop. The poles of the inner and outer, closed-loop systems are

$$\rho_p = \begin{bmatrix} -37.187 & -8.033 & -0.15 \end{bmatrix} \tag{8.9}$$

and

$$\rho = \begin{bmatrix} -37.16 & -8.03 & -0.137 & -0.015 & -0.0122 \pm 0.662 \end{bmatrix} \tag{8.10}$$

respectively.

The control scheme can thus be concluded to be stable. A simulation using this control scheme is shown in **figure 8.2**.

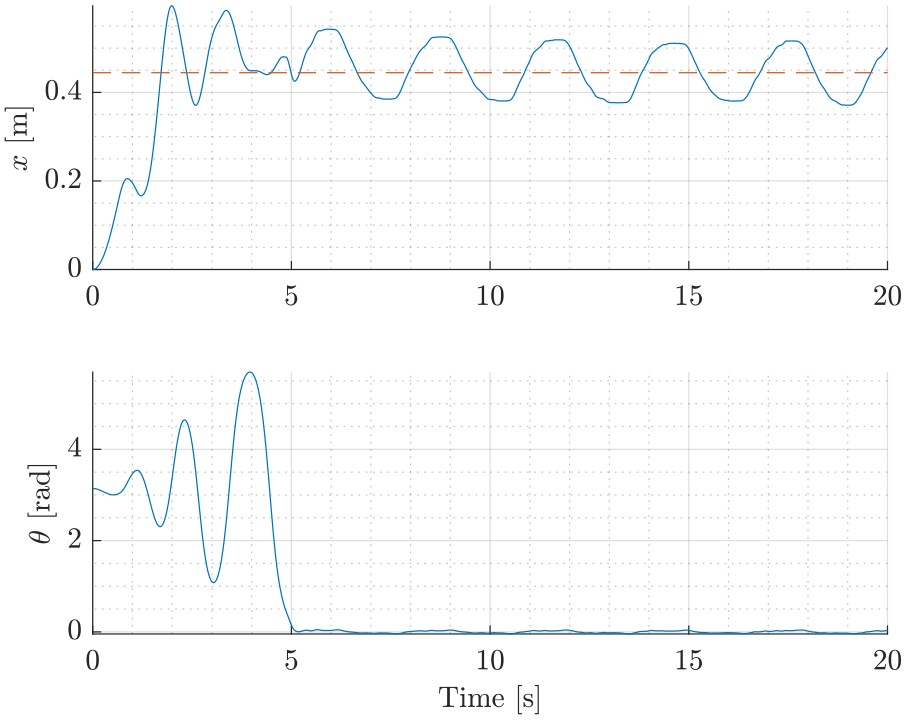

Figure 8.2: *PID simulation results on the full nonlinear model. The dotted red line, on the top figure, indicates the cart reference, x^*.*

The Mean Square Error (MSE) of the cart position and pendulum angle, from 10 seconds and until the end of the simulation is

$$\text{MSE}_c = 2.791 \cdot 10^{-3} \text{ m}$$

$$\text{MSE}_p = 586.8 \cdot 10^{-3} \text{ rad}$$

The values of the MSEs reflect how the cart moves ± 5 cm around the reference, and the pendulum angle moves around the zero reference with ± 0.04 rad. The results are thus satisfactory, which concludes the PID design.

8.2 Linear-Quadratic-Gaussian regulator

The LQG control scheme consists of an Linear-Quadratic Regulator (LQR) which utilizes the EKF as the state estimator, and thus requires a linear state space model, i.e.

$$\begin{aligned} \dot{\mathbf{x}} &= \mathbf{A}\mathbf{x} + \mathbf{B}u \\ \mathbf{y} &= \mathbf{C}\mathbf{x} + \mathbf{D}u \end{aligned} \tag{8.11}$$

where, in this case, $\mathbf{C} = \mathbf{I}$, and $\mathbf{D} = 0$.

The matrices $\mathbf{A}$ and $\mathbf{B}$ are obtained by linearising the nonlinear system dynamics in **equation (4.40)**, that is

$$\dot{\mathbf{x}} = f(\mathbf{x}) + g(\mathbf{x})u \tag{8.12}$$

at $\theta = 0$, which yields

$$\mathbf{A} = \left.\frac{\partial f(\mathbf{x})}{\partial \mathbf{x}}\right|_{\theta=0} = \begin{bmatrix} 0 & 0 & 1 & 0 \\ 0 & 0 & 0 & 1 \\ 0 & \frac{m_p g}{m_c} & 0 & -\frac{v_\theta}{l m_c} \\ 0 & \frac{(m_c+m_p)g}{l m_c} & 0 & -\frac{(m_c+m_p)v_\theta}{l^2 m_p} \end{bmatrix} \tag{8.13}$$

and

$$\mathbf{B} = \left.\frac{\partial g(\mathbf{x})}{\partial u}\right|_{\theta=0} = \begin{bmatrix} 0 & 0 & \frac{1}{m_c} & \frac{1}{l m_c} \end{bmatrix}^T \tag{8.14}$$

have been found. The LQG control scheme is depicted in **figure 8.3**.

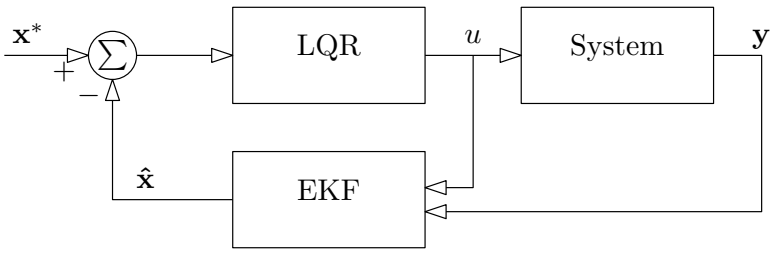

Figure 8.3: *The LQG control scheme, consisting of the LQR and the EKF, and System indicates the full model.*

The LQR is an optimal controller which minimizes an infinite horizon quadratic cost function given by

$$J = \int_0^\infty (\mathbf{x}^T \mathbf{Q} \mathbf{x} + \mathbf{u}^T \mathbf{R} \mathbf{u}) dt \tag{8.15}$$

The matrices $\mathbf{Q}$ and $\mathbf{R}$ are weighing matrices on the states and input, respectively. The weighing matrices are bounded by $\mathbf{Q} = \mathbf{Q}^T \geq 0$ and $\mathbf{R} = \mathbf{R}^T > 0$. The input u which minimizes J is

$$u = -\mathbf{k}\mathbf{x} \tag{8.16}$$

where $\mathbf{k}$ is given by

$$\mathbf{k} = \mathbf{R}^{-1}(\mathbf{B}^T \mathbf{P}) \tag{8.17}$$

and $\mathbf{P}$ is found by the solution to the algebraic Riccati equation

$$\mathbf{A}^T \mathbf{P} + \mathbf{P}\mathbf{A} - (\mathbf{P}\mathbf{B})\mathbf{R}^{-1}(\mathbf{B}^T \mathbf{P}) + \mathbf{Q} = 0 \tag{8.18}$$

The weighing matrices $\mathbf{Q}$ and $\mathbf{R}$ are design dependent. A good initial choice of weights can be determined by using Bryson's rule which defines the diagonal elements of the matrices as

$$\mathbf{Q}_{(k,k)} = \frac{1}{(x_k)^2_{max}}, \qquad k = 1, ..., n, \quad n = \dim \mathbf{x} \tag{8.19}$$

$$\mathbf{R} = \frac{1}{u^2_{max}} \tag{8.20}$$

Applying Bryson's rule normalizes the weigths which is benefical since they have different units. The weights for the cart and pendulum states are based on the requirements defined in **sections 3.1.1** and **3.1.2**, i.e. the pendulum is required to be ± 0.05 radians from zero, and the cart ± 10 cm from the centre:

$$\mathbf{Q}_{(2,2)} = \mathbf{Q}_{(4,4)} = \frac{1}{0.05^2} = 400 \tag{8.21}$$

$$\mathbf{Q}_{(1,1)} = \mathbf{Q}_{(3,3)} = \frac{1}{0.1^2} = 100 \tag{8.22}$$

The maximum deviation of input is set to 10 N which results in the following weight

$$\mathbf{R} = \frac{1}{10^2} = 0.01 \tag{8.23}$$

By choosing $\mathbf{Q}$ to be diagonal individual weighing on the states are achieved. Using the MATLAB function `lqr` with the above weights, the gain vector is found as

$$\mathbf{k} = \begin{bmatrix} -100 & 1012 & -172.1 & 266.8 \end{bmatrix} \tag{8.24}$$

To ensure stability, the eigenvalues of the closed-loop system $\mathbf{A} - \mathbf{Bk}$ must have negative real parts, and are found by solving $\det(\lambda \mathbf{I} - (\mathbf{A} - \mathbf{Bk})) = 0$ for λ, which gives

$$\lambda = \begin{bmatrix} -127.86 & -1.68 \pm 0.014i & -0.01 \end{bmatrix} \tag{8.25}$$

A simulation run with the above control gives the results in **figure 8.4**.

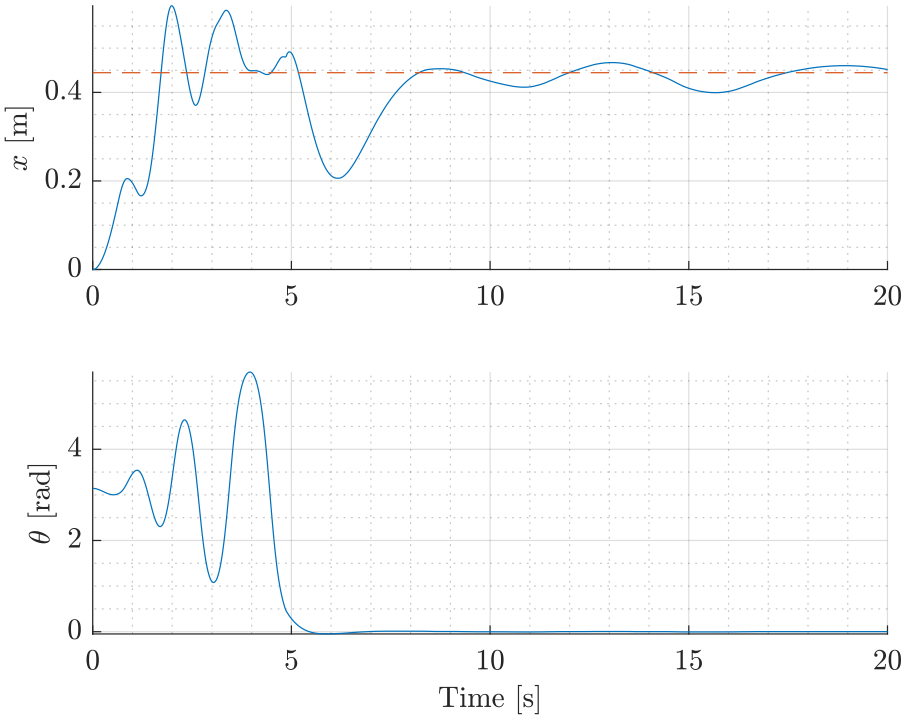

Figure 8.4: *LQG simulated on the full nonlinear model. The dotted red line in the top figure indicates the cart reference, x^*.*

The MSE of the cart position and pendulum angle, from 10 seconds until the end of the simulation is

$$\text{MSE}_c = 521.9 \cdot 10^{-6} \text{ m}$$

$$\text{MSE}_p = 9.460 \cdot 10^{-6} \text{ rad}$$

The cart moves ± 3 cm around the reference, and the pendulum is ± 0.005 rad from being completely upright, which the low MSE results indicate.

8.3 Sliding-Mode Controller

The following is based on [4].

The SMC is a nonlinear controller which is characterised by its way of leading the system states towards a *sliding manifold* and then along it until the manifold has converged to zero, as illustrated in **figure 8.5**.

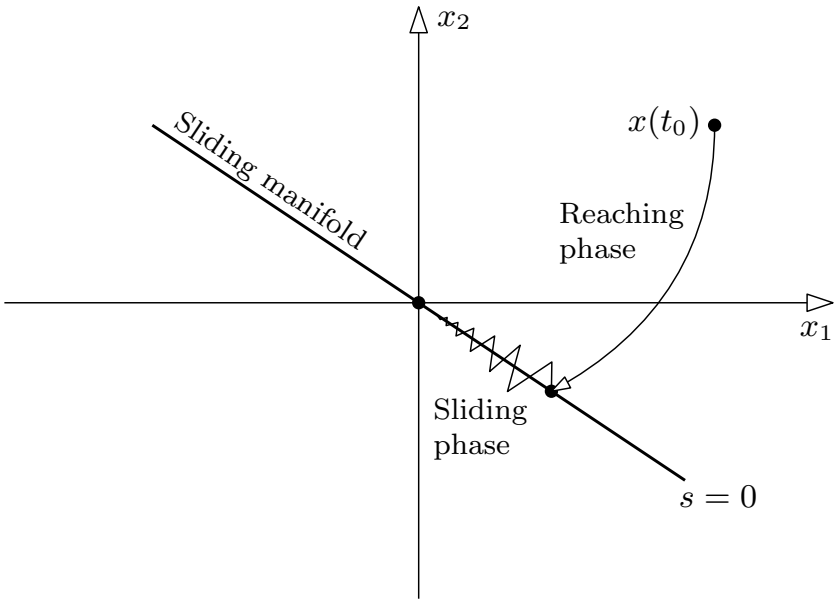

Figure 8.5: *Sliding-mode controller principle*

This is achieved by use of a system model, such that the system dynamics are compensated for, and the sliding manifold can be reached in finite time.

Considering the inverted pendulum system state vector $\mathbf{x} = [x_1 \quad x_2 \quad x_3 \quad x_4]^T = [x \quad \theta \quad \dot{x} \quad \dot{\theta}]^T$ with $n = 4$ states and $p = 1$ input, the sliding mode control design is based on the coordinate transformation $T: \ D \to R^n$

$$T(\mathbf{x}) = \begin{bmatrix} x_2 \\ x_3 \dfrac{\cos x_2}{l} - x_4 \\ x_1 - x^* \\ - - - - - \\ x_4 \end{bmatrix} = \begin{bmatrix} \eta_1 \\ \eta_2 \\ \eta_3 \\ \xi \end{bmatrix} = \begin{bmatrix} \eta \\ - - - \\ \xi \end{bmatrix}, \qquad \eta \in \mathbb{R}^{n-p}, \ \xi \in \mathbb{R}^p \tag{8.26}$$

$T(\mathbf{x})$ transforms the system from the form in **equation (4.40)**, i.e.

$$\dot{\mathbf{x}} = \begin{bmatrix} \dot{x} \\ \dot{\theta} \\ -\alpha(\mathbf{x}) - \beta(\mathbf{x}) \\ -\gamma(\mathbf{x}) - \delta(\mathbf{x}) \end{bmatrix} + \begin{bmatrix} 0 \\ 0 \\ \left(m_c + m_p \sin^2\theta\right)^{-1} \\ \cos\theta \left(l(m_c + m_p \sin^2\theta)\right)^{-1} \end{bmatrix} u \quad = \begin{bmatrix} \dot{x} \\ \dot{\theta} \\ f_c(\mathbf{x}) \\ f_p(\mathbf{x}) \end{bmatrix} + \begin{bmatrix} 0 \\ 0 \\ g_c(\mathbf{x}) \\ g_p(\mathbf{x}) \end{bmatrix} u \tag{8.27}$$

$$= f(\mathbf{x}) + g(\mathbf{x})u$$

into the *regular form*:

$$\begin{bmatrix} \dot{\eta} \\ \dot{\xi} \end{bmatrix} = \begin{bmatrix} f_a(\mathbf{x}) \\ f_b(\mathbf{x}) + g_b(\mathbf{x})u \end{bmatrix} = \frac{\partial T(\mathbf{x})}{\partial \mathbf{x}} f(\mathbf{x}) + \frac{\partial T(\mathbf{x})}{\partial \mathbf{x}} g(\mathbf{x})u \tag{8.28}$$

with

$$\frac{\partial T(\mathbf{x})}{\partial \mathbf{x}} = \begin{bmatrix} 0 & 1 & 0 & 0 \\ 0 & -\dfrac{\sin x_2}{l} & \dfrac{\cos x_2}{l} & -1 \\ 1 & 0 & 0 & 0 \\ 0 & 0 & 0 & 1 \end{bmatrix} \tag{8.29}$$

$$\frac{\partial T(\mathbf{x})}{\partial \mathbf{x}} f(\mathbf{x}) = \begin{bmatrix} x_4 \\ -x_4 \dfrac{\sin x_2}{l} + \beta(\mathbf{x}) \left(\dfrac{1 + \frac{m_c}{m_p} - \cos^2\theta}{\cos\theta} \right) \\ x_3 \\ f_p(\mathbf{x}) \end{bmatrix} \tag{8.30}$$

$$\frac{\partial T(\mathbf{x})}{\partial \mathbf{x}} g(\mathbf{x}) = \begin{bmatrix} 0 & 0 & 0 & g_p(\mathbf{x}) \end{bmatrix}^T \tag{8.31}$$

In (η, ξ)-coordinates, $f_a(\eta, \xi)$ and $f_b(\eta, \xi)$ then become:

$$f_a(\eta, \xi) = \begin{bmatrix} \xi \\ -\xi \dfrac{\sin\eta_1}{l} + \beta(\eta, \xi) \left(\dfrac{1 + \frac{m_c}{m_p} - \cos^2\eta_1}{\cos\eta_1} \right) \\ \dfrac{l}{\cos\eta_1}(\eta_2 + \xi) \end{bmatrix} \tag{8.32}$$

$$f_b(\eta, \xi) = f_p(\eta, \xi) \tag{8.33}$$

From this, a sliding manifold $s = \xi - \phi(\eta) = 0$ is designed such that

$$\dot{\eta} = f_a(\eta, \phi(\eta)) \tag{8.34}$$

has an asymptotically stable equilibrium point at the origin when motion is restricted to the manifold.

A linear design of $\phi(\eta)$, i.e.

$$\phi(\eta) = -\mathbf{k}\eta, \qquad \mathbf{k} = \begin{bmatrix} k_1 & k_2 & k_3 \end{bmatrix} \tag{8.35}$$

is achieved by pole placement for the closed-loop system in regular form, linearised in $\eta = \xi = 0$, that is

$$\dot{\eta}_{lin} = \mathbf{A}\eta + \mathbf{B}\phi(\eta) \tag{8.36}$$

with

$$\mathbf{A} = \left.\frac{\partial f_a(\eta,\xi)}{\partial \eta}\right|_{\eta=\xi=0} = \begin{bmatrix} 0 & 0 & 0 \\ -\frac{g}{l} & 0 & 0 \\ 0 & l & 0 \end{bmatrix} \tag{8.37}$$

$$\mathbf{B} = \left.\frac{\partial f_b(\eta,\xi)}{\partial \xi}\right|_{\eta=\xi=0} = \begin{bmatrix} 1 & \frac{v_{p,lin}}{l^2 m_p} & l \end{bmatrix}^T \tag{8.38}$$

which is controllable as its controllability matrix has full rank. Note that for the computation of $\mathbf{A}$ and $\mathbf{B}$, the system has been assuming to only have viscous friction terms, hence $v_{p,lin}$, in order to avoid dependency on the slope coefficient k in $\tanh(k\dot{\theta})$.

The desired closed-loop poles are chosen to be -1 and $-4 \pm 2.4j$, and found via the MATLAB-function `place`, which yields the gain vector

$$\mathbf{k} \approx [10 \quad -1 \quad -2] \tag{8.39}$$

From this, the sliding manifold becomes

$$\begin{aligned} s &= \xi - \phi(\eta) = \xi + \mathbf{k}\eta \\ &= \xi + k_1\eta_1 + k_2\eta_2 + k_3\eta_3 \\ &= \dot{\theta} + k_1\theta + k_2\left(\dot{x}\frac{\cos\theta}{l} - \dot{\theta}\right) + k_3(x - x^*) \end{aligned} \tag{8.40}$$

To find the sliding-mode control law, the time derivative of **equation (8.40)** is taken in order to obtain an explicit dependency of the input u:

$$\begin{aligned} \dot{s} &= \ddot{\theta} + k_1\dot{\theta} + k_2\frac{d}{dt}\left(\dot{x}\frac{\cos\theta}{l} - \dot{\theta}\right) + k_3(\dot{x}) \\ &= \ddot{\theta} + k_1\dot{\theta} + k_2\left(\ddot{x}\frac{\cos\theta}{l} - \dot{x}\frac{\sin\theta}{l} - \ddot{\theta}\right) + k_3(\dot{x}) \\ &= f_p(\mathbf{x}) + g_p(\mathbf{x})u + k_1\dot{\theta} + k_2\left(\left(f_c(\mathbf{x}) + g_c(\mathbf{x})u\right)\frac{\cos\theta}{l} - \dot{x}\frac{\sin\theta}{l} - f_p(\mathbf{x}) + g_p(\mathbf{x})u\right) + k_3(\dot{x}) \\ &= \underbrace{(1-k_2)f_p(\mathbf{x}) + k_2 f_c(\mathbf{x})\frac{cos\theta}{l} + k_1\dot{\theta} + \left(k_3 - k_2\frac{\sin\theta}{l}\right)\dot{x}}_{\Phi} + \underbrace{\left((1-k_2)g_p(\mathbf{x}) + k_2 g_c(\mathbf{x})\frac{\cos\theta}{l}\right)}_{\Gamma} u \end{aligned} \tag{8.41}$$

The control law is then defined as

$$u = -\Gamma^{-1}(\Phi + \lambda\,\mathrm{sgn}\,(s)), \qquad \lambda = \left|\frac{\Phi}{\Gamma}\right| + \lambda_0, \quad \lambda_0 > 0 \tag{8.42}$$

In order to validate the stability of this control law, consider the Lyapunov function candidate

$$V(s) = \frac{1}{2}s^2 \tag{8.43}$$

with time derivative

$$\begin{aligned}\dot{V}(s) &= s\dot{s} \\ &= s(\Phi + \Gamma u) \\ &= s\left(\Phi - \Gamma\Gamma^{-1}(\Phi + \lambda \operatorname{sgn}(s))\right) \\ &= s\left(\Phi - \Phi - \lambda \operatorname{sgn}(s)\right) \\ &= -s\lambda \operatorname{sgn}(s)\end{aligned} \tag{8.44}$$

Since $\operatorname{sgn}(s) = |s|\, s^{-1}$ for $s \neq 0$,

$$\dot{V}(s) = \begin{cases} -|s|\,\lambda < 0 & \text{for } s \neq 0 \\ 0 & \text{for } s = 0 \end{cases} \tag{8.45}$$

which, according to **theorem 6.1.1** (Lyapunov's stability theorem), shows that $s = 0$ is an asymptotically stable equilibrium point. Thus, trajectories starting outside $s = 0$ will reach the manifold in finite time and stay there. A simulation using this control is shown in **figure 8.6**.

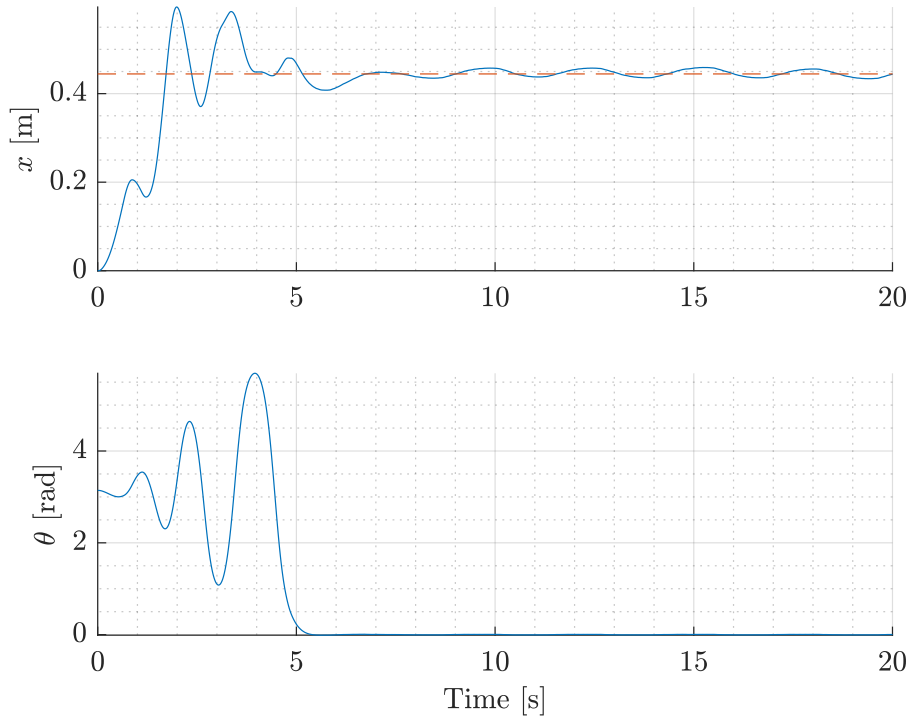

Figure 8.6: *Sliding-mode simulation results on the full nonlinear model. The dotted red line in the top figure indicates the cart reference, x^*.*

The MSE of the cart position and pendulum angle, from 10 s until the end of the simulation is

$$\text{MSE}_c = 65.51 \cdot 10^{-6} \text{ m}$$

$$\text{MSE}_p = 14.33 \cdot 10^{-6} \text{ rad}$$